Available online at www.sciencedirect.com

ScienceDirect

Procedia Engineering 109 (2015) 492 – 506

Procedia Engineering

www.elsevier.com/locate/procedia

XXIII Italian Group of Fracture Meeting, IGFXXIII

A numerical failure analysis of multi-bolted joints in FRP laminates based on basalt fibers

Francesca Nerilli[a,*], Michele Marino[b], Giuseppe Vairo[c]

[a] *Università degli Studi Niccolò Cusano - Telematica Roma, Via Don C. Gnocchi 13, 00166 Rome, Italy*
[b] *Leibniz Universität Hannover, Institute of Continuum Mechanics, Appelstr. 11, 30167 Hannover, Germany*
[c] *Università degli Studi di Roma "Tor Vergata", DICII, via del Politecnico 1, 00133 Rome, Italy*

Abstract

This paper aims to model the progressive damage of multi-bolted joints connecting structural elements made up of FRP (fiber-reinforced polymers) composite laminates and comprising different fiber materials (namely, based on basalt, carbon and glass), as well as different stacking sequences. Differences in failure mode and ultimate-load values are numerically investigated. A numerical home-made finite element model has been conceived, implemented, and validated by means of available experimental data. The numerical model is based on an incremental displacement-based approach and on a plane-stress bi-dimensional formulation. The stress analysis has been performed by accounting for micro-structural stress-strain localization mechanisms, and describing the progressive damage process by implementing a failure criterion operating at the constituents' scale (namely, the Huang's criterion). Proposed results have highlighted that bolted joints based on basalt-FRP laminates and defined by a double-bolted configuration exhibited bearing failure loads comparable to those computed for glass-FRP and carbon-FRP laminates. In the case of single-bolted joints, the use of carbon-FRP laminates allowed to obtain the best mechanical properties, although joints based on basalt-FRP laminates numerically-experienced mechanical response and strength features always comparable with those of glass-FRP.

Peer-review under responsibility of the Gruppo Italiano Frattura (IGF)

Keywords: Bolted joints; FRP composite laminates; Basalt fibers; Pin-bearing failure.

1. Introduction

Composite materials are nowadays widely spread in many structural fields, such as aerospace, industrial, automotive and civil applications, because of their high stiffness-to-weight and strength-to-weight ratios. Nevertheless, in order to achieve specific geometries and structural features, structural elements made up of composite materials generally need to be connected. Since the possible stress concentrations arising at the joint regions, associated also with the material heterogeneous microstructure, a fundamental task is related to the analysis of strength features for such joined structural systems. For instance, composite panel elements (namely, laminates) are joined to obtain specific

* Corresponding author. Tel.: +39-(0)6-7259-7088 ; fax: +39-(0)6-7259-7042.
E-mail address: francesca.nerilli@unicusano.it, marino@ikm.uni-hannover.de, vairo@ing.uniroma2.it

Peer-review under responsibility of the Gruppo Italiano Frattura (IGF)
doi:10.1016/j.proeng.2015.06.255

functional surfaces in aerospace and aeronautic applications; pultruded composite beams or columns are connected together to realize truss structures in civil applications. Composite elements are usually joined through bolted connections, adhesive binding, or by adhesive/bolted hybrid joints. Referring to the case of laminates joined via bolted connections, failure modes under tensile loads can usually occur following four different basic modes, namely, cleavage, net-tension, shear-out and bearing [1], whose activation is strongly related to both geometric (bolt diameter, laminate width and thickness, end-distance) and material properties (e.g., fiber-to-load angle, matrix and fiber type, laminate stacking sequence). In particular, for large enough width and end-distance of bolted laminates, bearing failure mode is generally dominant [1,2], consisting in a local laminate compressive failure induced by the tendency of the bolt to crush the composite material, with the local occurrence of matrix cracks. Due to the great relevance for design purposes, many researchers recently addressed pin-bearing failure mechanisms in bolted laminates. In detail, in this context many well-established experimental and numerical studies have been carried out aiming to give comparative indications on the bearing strength as a function of the fastener features (e.g., bolt diameter) [3], of the joint geometry (e.g., plate width and thickness), of the end-distance [4], of the laminate stacking sequence[5], of the mechanical properties of the composite material (e.g., matrix type and fiber nature), of the loading direction [6,7]. An useful overview of bearing failure mechanisms, supplied in a technical context and oriented towards a critical analysis of the current design practice, can be found in [8,9]. Moreover, the mechanical response of multi-bolted composite laminates has been recently addressed in [10,11], where special reference is made to load partition features and stress distribution mechanisms induced by these type of connections.

In the context of composite materials, fiber-reinforced polymers (FRP) based on fibers produced by molten basalt rock (in the following denoted as BFRP) has gained an increasing interest in the last years, as a result of the good physico-chemical properties that can be achieved with basalt, especially if compared with traditional glass and carbon fibers [12–15]. In fact, basalt fibers exhibit good strength and stiffness properties also at high temperatures, long-term durability, high acid and solvent resistance, low water absorbtion, remarkable heat and sound insulation properties, good processability, as well as their fabrication process is generally significantly cheaper than carbon and glass fibers. Moreover, basalt is widely available in nature with certain chemical and mineralogical composition, it has a non-toxic reaction with air or water, is non-combustible, is explosion-proof, and it is generally characterized by high levels of eco-compatibility and recyclability, resulting a high-performance green inorganical material. Therefore, basalt fibers and composite materials made from them attractively combine very interesting properties in terms of mechanical quality and cost in comparison with other types of fibers such as glass and carbon fibers [16].

In this paper the bearing failure mode of bolted joints in BFRP laminates is addressed through a numerical approach, aiming to establish quantitative comparisons with the case of glass fiber-reinforced (GFRP) and carbon fiber-reinforced (CFRP) laminates. In detail, starting from the nonlinear finite-element formulation proposed in [2,17] for the analysis of the elasto-damage problem in object, the numerical model has been enhanced in order to account for general laminate stacking sequences as well as for multi-bolted configurations. The numerical tool has been successfully validated by referring to available experimental data [5–7] and it has been proved to be able to furnish useful indications towards proper definition of possible technical design standards for bolted joints involving also BFRP laminates.

The paper is organized as follows. After a brief description in Section 2 of the main properties characterizing basalt fibers and composite materials made from them, the basic theoretical ingredients employed to establish the progressive damage model are described in Section 3, tracing the main lines of both numerical formulation and implementation algorithm. In Section 4 some preliminary validation results are presented. Comparative strength analyses of bolted laminates based on different fiber materials (namely, involving BFRP, GFRP and CFRP), laminate stacking sequences, and joint configurations are illustrated and discussed in Section 5. Finally, some conclusions are traced in Section 6.

2. Basalt fiber-reinforced composites

Within the framework of modern advanced composite materials, one of the most important type, from a structural point of view, is the fiber-reinforced type. In this case, the use of fibers with specific physical properties and arranged following suitable patterns within an embedding matrix, allows to design functional materials characterized by desired levels of strength and stiffness, combined with effective chemical and physical properties. Matrix is generally consti-

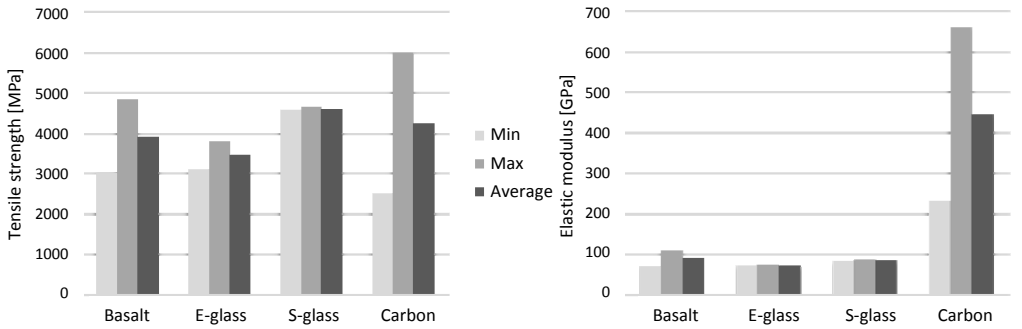

Fig. 1. Maximum, minimum and average values of (on the left) tensile strength and (on the right) elastic modulus reported in literature and measured in standard conditions for basalt, glass and carbon fibers [14,16,19].

tuted by polymeric resins (e.g., epoxy, vinylester), and fibers are usually based on glass, carbon, aramid compounds, although other fibers can be sometimes used.

Nowadays, the need to use and to develop sustainable composites, reinforced with natural fibers, is carefully considered in both research and manufacturing scenarios. In this field, basalt fibers are considered very attractive because of their low cost and their good mechanical properties. Basalt is a dark-coloured mafic extrusive rock and it is the most widespread of all igneous rocks, comprising more than 90% of all volcanic rocks. The cooling rate of molten lava strongly influences the microstructure of this rock: when the rate is low, basalt structure exhibits an almost regular atomic arrangement, while an amorphous (uncrystallized) structure arises when the solidification rate is high. The first attempts to transform basalt rock into fibers by extrusion started at the beginning of the 1920's and were attributed to the French Paul Dhè, that was granted a U.S. Patent in 1922 [18]. Around 1960, Soviet Union began to investigate basalt fiber applications too, particularly for military and aerospace purposes, succeeding in developing the first attempt of production technology for continuous basalt fibers. In subsequent years many technical studies have been conducted in Europe and more recently in China, aiming to improve quality of the manufacturing process as well as to enhance the physico-chemical features and mechanical performance of basalt fibers [16]. Actually, basalt fibers can be produced by means of two different technologies, namely the *Spinneret* technology and the *Junkers* one [14]. The first is generally used to produce continuous fibers, whereas the latter allows to obtain short fibers.

Like glass and carbon fibers, basalt fibers exhibit a mechanical response in tension that can be suitably described, within a certain strain range, as linearly elastic. For the sake of comparison, Fig.1 summarizes mean values of mechanical properties reported in literature for basalt fibers (in terms of elastic modulus and tensile strength) compared with those relevant to usually-employed glass and carbon fibers. It can be noted that the tensile strength of basalt fibers is generally characterized by average values very close to those of glass and carbon fibers. Moreover, although carbon fibers experience the greatest values of the elastic modulus, basalt fibers show stiffness values comparable to those of glass fibers (both E-glass and S-glass type). Furthermore, many experimental tests confirm a good thermo-chemical stability and promising mechanical properties of basalt fibers undergoing extreme values of temperature (in the range -300 to 700 ° C), chemical attacks, and aging processes [12–15].

As regards composites based on basalt fibers, special reference can be made to BFRP (basalt fiber-reinforced polymers). Their mechanical properties generally depends on the fiber pattern and fiber type (long or short), on the matrix characteristics, on the fiber content, as well as on the chemical bond arising among fibers and matrix. Referring to BFRP laminates, generally based on the use of long basalt fibers, many references can be found in literature that propose comparative experimental results among mechanical performances of BFRP, GFRP and CFRP laminates. As an example, a comparison between basalt and glass fiber-reinforced epoxy composites was investigated in [20], highlighting that the elastic stiffness estimated for BFRP laminates is higher, almost independently on the mechanical test (tensile, compression or bending test), than that of GFRP laminates up to 35 – 40 %, and that bearing load values experienced for BFRP laminates are greater or at least comparable to those obtained for GFRP. Similarly, experimental results proposed in [21,22], and obtained for BFRP, GFRP and CFRP laminates comprising the same polymeric matrix and the same fiber content, confirm that BFRP laminates exhibit a tensile strength close to that of GFRP's, but lower than that of CFRP's, and that they can generally experience high values of ultimate tensile strains. Finally, these

experimental data suggest that BFRP laminates are usually characterized by a better performance with respect to the fatigue behaviour in comparison with GFRP [21,22].

3. Progressive damage model

Let fiber-reinforced composite laminates be composed by the assembly of several thin layers (namely, plies), each one consisting in unidirectional continuous fibers embedded in a polymeric matrix, to form a plate-like structural element with a planar reference configuration. Fiber material is assumed to be linearly elastic and transversely isotropic, with symmetry plane orthogonal to the fiber axis, and matrix material is assumed to behave as an isotropic linearly elastic material. Accordingly, each ply turns out to be characterized by a linearly elastic transversely isotropic effective mechanical response, the fiber direction being a constitutive symmetry axis. Let FRP laminates herein analyzed be defined by a symmetric plying sequences, and characterized by a small side-to-thickness ratio. Moreover, a pin-based load transfer mechanism is herein modeled, neglecting any effect related to bolt preloading conditions. Accordingly, under the further assumption of zero out-of-plane loads acting upon the laminates, a plane-stress regime can be conveniently enforced in what follows.

As a notation rule, the superscript A indicates the fiber direction, T the transverse-to-the-fiber direction, and the apex sign $+/-$ distinguishes strength material properties in traction and compression, respectively. When necessary, the index c will discriminate the constituents at the microscale, that is $c = f$ for fibers and $c = m$ for the matrix. Moreover, $\mathcal{P}_k$ indicates the kth ply, and $(A, T)_k$ is the corresponding local in-plane reference system (aligned with the fiber direction). The undamaged matrix material is described by Young modulus E_m and Poisson ratio ν_m (with $G_m = E_m/[2(1+\nu_m)]$), and (in a local reference system) the undamaged fiber material is described by the engineering constants E_f^A, E_f^T, G_f^{AT}, ν_f^{AT}, ν_f^T. The pins are assumed to be characterized by a linearly elastic isotropic material (E_p and ν_p being the corresponding elastic constant), not experiencing damage effects.

In order to describe pin-bearing damage initiation and growth in bolted joints of FRP laminates, a progressive damage modeling technique is herein employed. In the framework of an incremental approach, at each incremental step a proper stress analysis is performed by using an homogenization procedure. Afterwards, stress patterns estimated in each ply are used to establish possible failure mechanisms on the basis of strength criteria applied to FRP layers. Finally, a suitable material degradation law is introduced to account for failure occurrence in composite constituents at the microscale.

3.1. Stress analysis

The mechanics of FRP laminates is herein described by considering the classical laminate theory [23–25], combined with the *bridging model* [17,26] as an homogenization procedure that allows one to describe localization mechanisms. In detail, by referring to a displacement-driven incremental approach, and by employing a standard Voigt notation, the use of the laminate theory allows to compute the homogenized in-plane strain increment field $d\boldsymbol{\varepsilon}$ for the laminate. Therefore, the homogenized in-plane stress increment field in $\mathcal{P}_k$ is

$$d\boldsymbol{\sigma}_k = (\mathcal{S})_k^{-1}(d\boldsymbol{\varepsilon})_k\,, \tag{1}$$

where $(d\boldsymbol{\varepsilon})_k = \{d\varepsilon_{11}\ \ d\varepsilon_{22}\ \ d\varepsilon_{12}\}^t$ denotes the local-to-$\mathcal{P}_k$ representation of $d\boldsymbol{\varepsilon}$, with indexes 1 and 2 corresponding to A and T directions, respectively. Moreover, the equivalent 3×3 in-plane compliance matrix $(\mathcal{S})_k$ computed in $(A, T)_k$ results in [26]:

$$(\mathcal{S})_k = \left\{V_f(\mathcal{S}^f)_k + V_m\mathcal{S}^m(\mathcal{A})_k\right\}\left\{V_f\mathcal{I} + V_m(\mathcal{A})_k\right\}^{-1} \tag{2}$$

where $\mathcal{I}$ denotes the identity matrix, and V_f (respectively, V_m) is the fiber (resp., matrix) volume fraction (thereby, $V_m = 1 - V_f$), herein assumed to be the same for all plies $\mathcal{P}_k$. Moreover, $(\mathcal{S}^c)_k$ is the local-to-$\mathcal{P}_k$ in-plane compliance matrix for the constituent c, and $(\mathcal{A})_k$ is the local-to-$\mathcal{P}_k$ in-plane bridging linear operator. By omitting for the sake of

compactness the index k, the latter is component-wise defined through:

$$\mathcal{A}_{11} = \frac{E_m}{E_f^A}, \qquad \mathcal{A}_{22} = \frac{1}{2}\left(1 + \frac{E_m}{E_f^T}\right), \qquad \mathcal{A}_{22} = \frac{1}{2}\left(1 + \frac{G_m}{G_f^T}\right), \qquad \mathcal{A}_{21} = \mathcal{A}_{31} = \mathcal{A}_{32} = 0, \tag{3}$$

$$\mathcal{A}_{12} = \frac{\mathcal{S}_{12}^f - \mathcal{S}_{12}^m}{\mathcal{S}_{11}^f - \mathcal{S}_{11}^m}\left(\mathcal{A}_{11} - \mathcal{A}_{22}\right), \qquad \mathcal{A}_{13} = \frac{d_2\beta_{11} - d_1\beta_{21}}{\beta_{11}\beta_{22} - \beta_{12}\beta_{21}}, \qquad \mathcal{A}_{23} = \frac{d_1\beta_{22} - d_2\beta_{12}}{\beta_{11}\beta_{22} - \beta_{12}\beta 21}, \tag{4}$$

where

$$d_1 = \mathcal{S}_{13}^m\left(\mathcal{A}_{11} - \mathcal{A}_{33}\right), \qquad d_2 = \mathcal{S}_{23}^m\left(V_f + V_m\mathcal{A}_{11}\right)\left(\mathcal{A}_{22} - \mathcal{A}_{33}\right) + \mathcal{S}_{13}^m\left(V_f + V_m\mathcal{A}_{33}\right)\mathcal{A}_{12}, \tag{5}$$

$$\beta_{11} = \mathcal{S}_{12}^m - \mathcal{S}_{12}^f, \qquad \beta_{12} = \mathcal{S}_{11}^m - \mathcal{S}_{11}^f, \qquad \beta_{22} = \left(V_f + V_m\mathcal{A}_{22}\right)\left(\mathcal{S}_{12}^m - \mathcal{S}_{12}^f\right), \tag{6}$$

$$\beta_{21} = V_m\left(\mathcal{S}_{12}^f - \mathcal{S}_{12}^m\right)\mathcal{A}_{12} - \left(V_f + V_m\mathcal{A}_{11}\right)\left(\mathcal{S}_{22}^f - \mathcal{S}_{22}^m\right). \tag{7}$$

In agreement with [26], by assuming that in each domain $\mathcal{P}_k$ the relationship $d\boldsymbol{\sigma}_k = V_f(d\boldsymbol{\sigma}_f)_k + V_m(d\boldsymbol{\sigma}_m)_k$ holds, where $(d\boldsymbol{\sigma}_c)_k = \{d\sigma_{11} \;\; d\sigma_{22} \;\; d\sigma_{12}\}_c^t$ denotes the local-to-$\mathcal{P}_k$ representation of $d\boldsymbol{\sigma}_c$, a measure of the stress increments for fibers and matrix in $\mathcal{P}_k$ result from:

$$(d\boldsymbol{\sigma}_f)_k = (\mathcal{B})_k d\boldsymbol{\sigma}_k, \qquad\qquad (d\boldsymbol{\sigma}_m)_k = (\mathcal{A})_k(\mathcal{B})_k\, d\boldsymbol{\sigma}_k, \tag{8}$$

where the local-to-$\mathcal{P}_k$ in-plane localization matrix is defined by

$$(\mathcal{B})_k = \left[V_f\mathcal{I} + V_m(\mathcal{A})_k\right]^{-1}. \tag{9}$$

3.2. Failure analysis

Failure mechanisms are herein assumed to be controlled by the stress field at the micro-scale. In fact, as numerically experienced in [17], the use of an approach able to account for localization mechanisms at the micro-scale and able to discriminate the damage occurrence for fiber and matrix constituents in each ply, allows one to furnish more accurate estimates of laminate strength properties than meso-scale criteria, such as that by Rotem [27].

In detail, reference is made to the biaxial strength criterion proposed by Huang [26]. Thereby, the constituent c of $\mathcal{P}_k$ is assumed to experience a tensile or compressive failure, respectively, if

$$\sigma_{eq,c} \geq S_c^+, \qquad \text{tensile failure condition} \tag{10}$$

$$\sigma_c^{(2)} \leq -S_c^-, \qquad \text{compressive failure condition} \tag{11}$$

where, omitting for the sake of compactness the index k, $\sigma_c^{(1)}$ and $\sigma_c^{(2)}$ are the actual values of the first (maximum) and the second (minimum) principal stresses for c in $\mathcal{P}_k$, $S_c^{+/-}$ denotes tensile (+) and compressive (-) constituent strength, and $\sigma_{eq,c}$ is defined as:

$$\sigma_{eq,c} = \begin{cases} \sigma_c^{(1)} & \text{if } \sigma_c^{(2)} \leq 0 \\ \left[\left(\sigma_c^{(1)}\right)^{q_c} + \left(\sigma_c^{(2)}\right)^{q_c}\right]^{1/q_c} & \text{if } \sigma_c^{(2)} > 0, \end{cases} \tag{12}$$

with q_c such that $1 < q_c < \infty$, being a power index, generally depending on the constituent c, that allows to account for biaxial stress effects on the bearing capacity.

3.3. Degradation rule

When the previously-introduced failure criterion is satisfied for the constituent c in a point of a certain ply $\mathcal{P}_k$ constituting the laminate, local material properties of c are assumed to undergo a mechanical degradation. A simple degradation law is herein employed by assuming that, when damage occurs, the elastic stiffness $(\mathcal{S}^c)^{-1}$ of the damaged constituent (fiber or matrix) reduces by the factor $\eta_c > 1$.

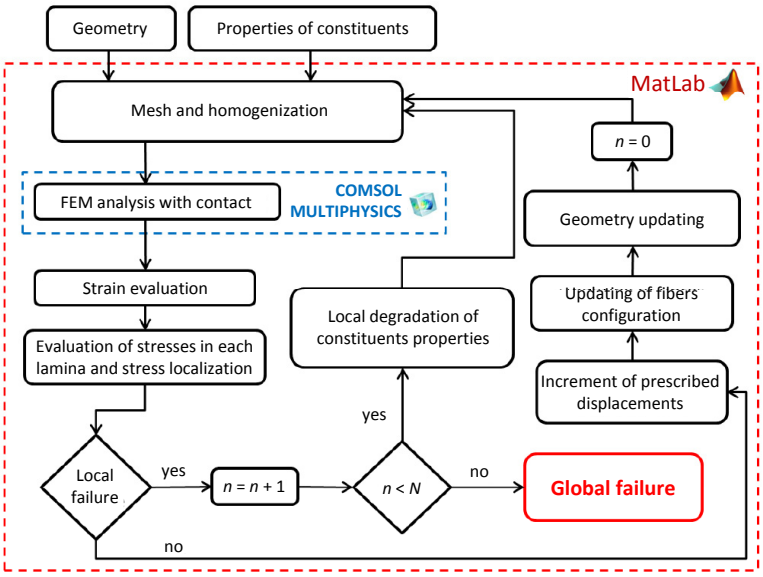

Fig. 2. Iterative algorithm implemented via an incremental finite-element approach and employed for describing the progressive damage of FRP bolted laminates. n denotes the iteration index within a single incremental step.

3.4. Numerical procedure

The in-plane elasto-damage incremental problem previously introduced is treated via a finite element (FE) formulation. The unilateral contact condition between laminate hole(s) (internal laminate boundary) and pin-bolt(s) is numerically described through a surface-to-surface penalty method, by neglecting any friction effect. The computational domain (comprising of both the laminate and pin-bolt(s)) is discretized by employing triangular finite elements, based on a pure displacement formulation with quadratic displacement shape functions. The numerical model is based on an incremental displacement approach, that can be driven both by the pin position or by prescribing suitable displacement conditions at the external laminate boundary. To this aim, a numerical iterative procedure, based on the algorithm briefly summarized in Fig. 2, has been implemented. In particular, a Matlab home-made code has been developed and integrated with the commercial solver Comsol Multyphysics for the finite-element computations and for managing the nonlinear contact at the pin-laminate interfaces.

Starting from the discretized model of both the punched FRP laminate and pin-bolt(s), and referring to undamaged constituents' properties, the constitutive features of each triangular element belonging to the laminate mesh are initialized by considering the equivalent homogenized material description obtained through the laminate theory and the afore-mentioned homogenization approach. At each incremental step, the laminate homogenized in-plane strain field results from the FE-based solution and, since Eqs. (1) and (8), the increment of the stress field in each layer $\mathcal{P}_k$ and in each constituent (fibers and matrix) are computed. Addressing the actual stress field on each ply, obtained by superimposing the corresponding stress increments, the failure criterion established in Section 3.2 is employed in order to verify possible damage occurrence. If local failure conditions are not detected then system geometry is updated, fibers packaging is updated on the basis of the computed strain field increment, and the value of the prescribed displacement is increased to perform the analysis of a new incremental step. Otherwise, if damage locally occurs for a certain constituent then the corresponding material properties are locally altered by employing the degradation law previously introduced. In order to check the occurrence of a possible progressive failure path at that step, the actual incremental step is repeated with the same geometry and under the same boundary conditions until further material failure is no longer detected in the overall computational domain. If this iterative procedure does not converge (i.e., referring to the notation introduced in Fig. 2, if the condition $n > N$ occurs, with $N \gg 1$ an assigned control parameter) the global failure condition is assumed to be reached. In this case and at the last converged incremental step, the

Table 1. Undamaged material properties [6,7,23,28] and other model parameters employed for the validation case 1.

Fiber					Matrix		
$S_f^{+/-}$ (GPa)	$E_f^A = E_f^T$ (GPa)	$\nu_f^T = \nu_f^{AT}$	G_f^{AT} (GPa)	V_f (%)	$S_m^{+/-}$ (MPa)	E_m (GPa)	ν_m
2.5	50.0	0.18	21.2	60	26.0	1.4	0.4
CSM			Pin		Other		
$S_{CSM}^{+/-}$ (MPa)	E_{CSM} (GPa)	ν_{CSM}	E_p (GPa)	ν_p	η	q_c	N
250.0	12.41	0.4	210.0	0.3	100	5	20

numerical integral of the distributed reaction force at the internal laminate boundary is considered as a measure of the corresponding failure load.

4. Preliminary validation results

In order to show soundness and consistence of the proposed numerical approach, preliminary validation analyses have been carried out. In detail, in the following reference is made to the experimental studies recently presented by Ascione et al. [6,7] (validation case 1) and to results proposed by Khashaba et al. [5] (validation case 2), also addressed in [17] and [2], respectively.

4.1. Validation case 1

The experimental tests established in [6,7] refer to a pin-plate system based on GFRP laminates, and give useful indications about the influence of the fiber-to-load angle α on the bearing failure load induced by a steel pin. In detail, with reference to the notation introduced in Fig. 3, the experimental test addressed in [6,7] is based on a pin-plate system comprising of a square plate (500 mm wide and 10 mm thick) consisting in eight equally-oriented plies of Continuous Strand Mat GFRP composite material placed between two CMS (Chopped Strand Mat) plies, resulting in the stacking sequence $[\mathrm{CSM}/0_4]_s$, with plies 1 mm thick each one. Due to the adopted experimental testing system [6,7], the problem is statically equivalent to consider a circular plate 300 mm in diameter (see Fig. 3), fully restrained on its external boundary. At the laminated plate center a circular hole of diameter $D = 20$ mm was considered, wherein a steel pin was inserted and acted upon by a testing load parallel to the plate along a direction inclined at the angle α with respect to the fiber direction. The case of a neat-fitting pin (i.e., zero clearance between hole and pin) is herein addressed, and the progressive damage is incrementally simulated as driven by the position of the pin center, assuming a pin-displacement increment of $10^{-2}D$. As a result of a preliminary convergence analysis, computational

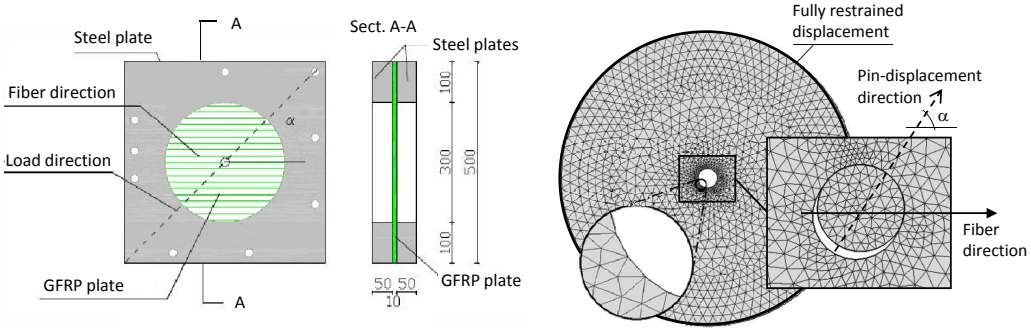

Fig. 3. Validation case 1. (a) GFRP-laminate sample tested in [6,7] (dimension in mm). (b) Mesh details and boundary conditions employed for numerical simulations.

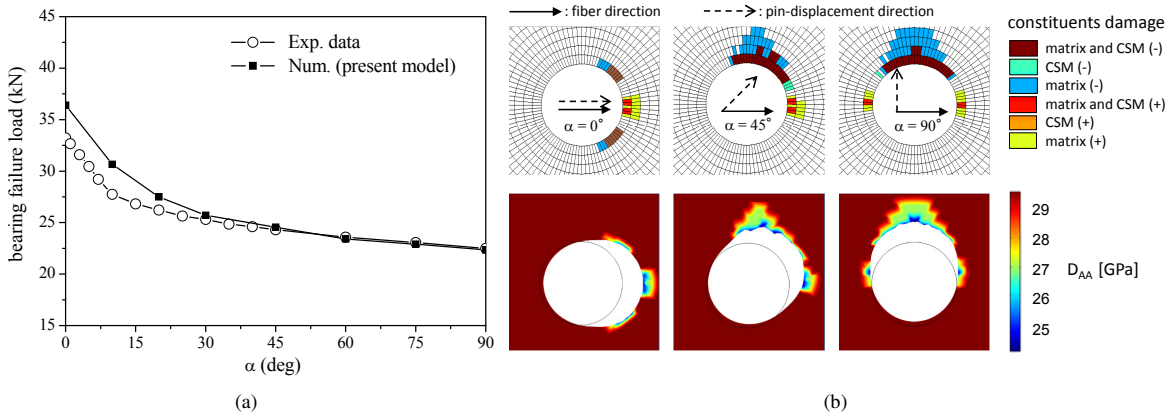

Fig. 4. Validation case 1. (a) Comparison among values of the bearing failure load predicted via the present model and those experimentally measured in [6,7], vs. the fiber-to-load angle α. (b) Numerical results, at the failure state and for different values of α, relevant to the damage occurrence in each composite constituents and to the patterns of the material degradation (on the deformed configuration). D_{AA} denotes the equivalent material stiffness of the entire laminate along the fiber direction.

mesh consisted in about 150.000 elements, with a mesh refinement close to the pin-plate interface characterized by an average mesh-size of about 0.1 D.

Results obtained by considering CSM as a linearly elastic isotropic material (since a CSM ply is made up of short glass fibers randomly dispersed inside the matrix), and referring to the values of model parameters summarized in Table 1, are synthetically depicted in Fig. 4. In particular, Fig. 4a shows the comparison between experimental values of the bearing failure load and those computed via the present approach, versus the fiber-to-load angle α. Proposed results are in good agreement with experimental-based data, highlighting the model capability to predict the failure-load sensitivity to the fiber-to-load angle. It is worth observing that, the little discrepancies observed for small values of α could be attributed to a more complex constitutive behaviour than the isotropic one of the CSM plies. Moreover, Fig. 4b reports the local damage scenarios numerically-experienced at the failure state for different values of α, discriminating in each ply the constituent that experiences damage. These results, obtained via a post-processing procedure involving a slave partition with respect to the computational mesh, confirm that damage occurs close to the pin-plate contact interface, mainly involving the damage of matrix and CSM. In Fig. 4b, patterns of the equivalent material stiffness for the entire laminate along the fiber direction (denoted as D_{AA}) are also shown, providing a further evidence of the damage localization at the failure state (blue color indicates a fully damaged point, brownish red undamaged regions). In agreement with experimental evidence, proposed results clearly suggest that when $\alpha = 0$ the failure mechanisms is mainly driven by the bearing mode, whereas when the fiber direction is orthogonal to the loading-transmission one the occurrence of the net-tension mode also occurs, although bearing effects remain dominant.

4.2. Validation case 2

In order to validate the proposed numerical model for laminates with stacking sequences that include differently oriented plies, a comparison with some experimental results reported in [5] has been carried out. In detail, the experimental campaign concerned pin-bearing tests, conducted on GFRP specimens with different stacking sequences. Reference is herein made to the experimental data relevant to a rectangular laminated plate (36 mm × 135 mm) 3.1 mm thick, comprising of eight plies (having the same thickness) with the symmetrical stacking sequence $[0\ 90]_{2s}$ (the fiber angle is defined with respect to the direction x aligned with the long side of the plate, see Fig. 5), based on E-glass fibers embedded in epoxy resin. At the end-distance $E = 18$ mm from one of the short side of the plate, a circular hole of diameter $D = 6$ mm was present, where a steel neat-fitting pin was inserted. At the opposite short side of the laminate an incremental displacement condition was applied.

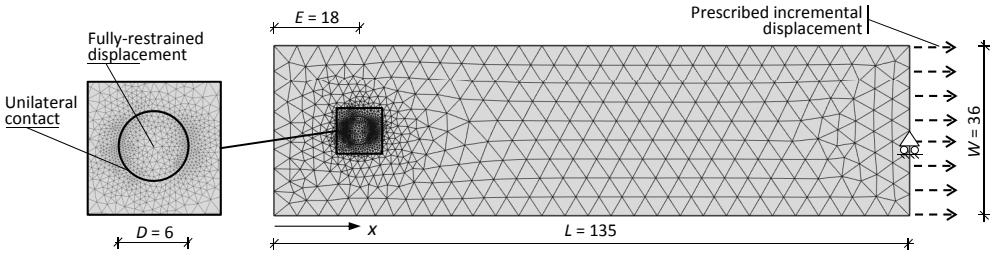

Fig. 5. Validation case 2. Geometry, mesh details and boundary conditions (dimension in mm), in agreement with [5].

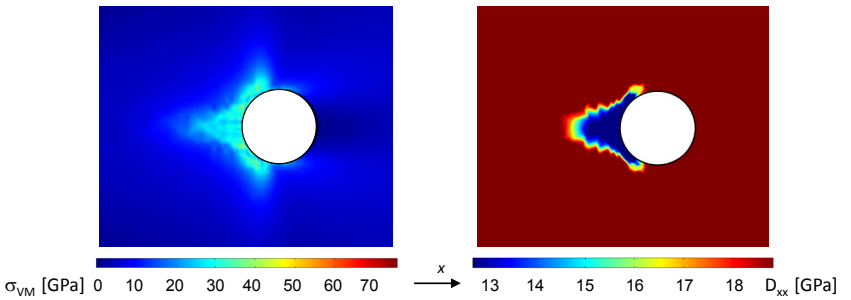

Fig. 6. Validation case 2. (Left) Von Mises stress (σ_{VM}) distribution and (right) equivalent material stiffness of the entire laminate along the direction x (denoted as D_{xx}) at the failure state and on the undeformed configuration, close to the pin-plate interface.

Model geometry adopted for numerical simulations and some mesh details are depicted in Fig. 5, highlighting also the mesh refinement around the pin-plate interface, characterized by an average mesh size of about $5 \times 10^{-2} D$. As boundary conditions, the pin center is assumed to be fully restrained, unilateral frictionless contact is considered at the pin-plate interface, and an incremental displacement condition is enforced at the right laminate edge, with the displacement increment assumed to be equal to $0.5 \times 10^{-2} D$. Table 2 summarizes the values of model parameters employed for numerical computations.

The failure load evaluated via the present model results in 4.15 kN, in a really good agreement with the experimental value of 4.2 kN. With reference to the failure state, attained following mainly a bearing mode and as a result of the matrix failure at the pin-laminate interface, the Fig. 6 depicts the distribution of the equivalent von Mises stress measure and the distribution of the equivalent material stiffness for the entire laminate along the direction x (denoted as D_{xx}), providing an evidence of the damage localization mechanisms at the pin-plate interface (blue color indicates a fully damaged point, brownish red undamaged regions).

5. Comparative analysis: influence of fiber material and pin number

In order to investigate about the influence of fiber material and pin number on the failure mechanisms and on the value of the failure load, a number of comparative numerical analyses have been performed.

Table 2. Undamaged material properties [5] and other model parameters employed for the validation case 2. Pin properties are the same as in Table 1.

Fiber					Matrix			Other		
$S_f^{+/-}$ (GPa)	$E_f^A = E_f^T$ (GPa)	$\nu_f^T = \nu_f^{AT}$	G_f^{AT} (GPa)	V_f (%)	$S_m^{+/-}$ (MPa)	E_m (GPa)	ν_m	η	q_c	N
3.45	72.4	0.22	29.7	40	69.0	3.2	0.36	100	3	10

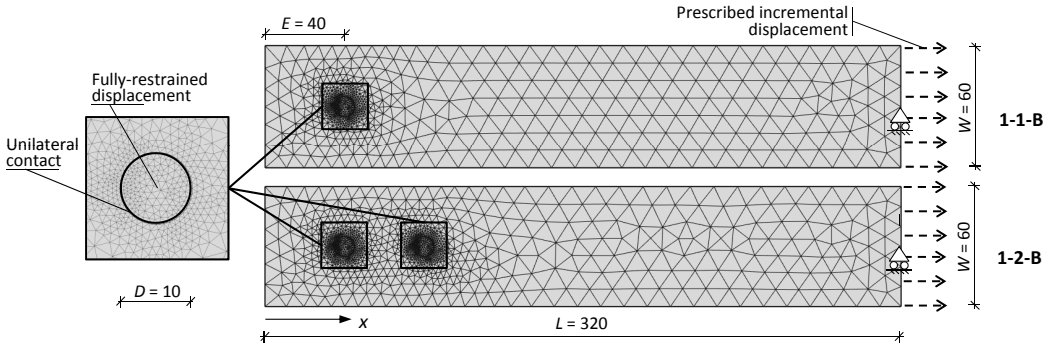

Fig. 7. Comparative analysis. Geometry, mesh details and boundary conditions (dimension in mm). 1-1-B: single-bolted joint configuration. 1-2-B: double-bolted joint configuration, with two pins along the loading direction x.

5.1. Problem statement

Laminates based on basalt (BFRP), carbon (CFRP) and glass (GFRP) fibers embedded in an epoxy resin as matrix, and defined by considering the same fiber volume fraction $V_f = 60\,\%$, have been analysed. Moreover, both the cases of single-bolted joints (one pin, referred to as 1-1-B) and double-bolted joints (two pins, aligned along the loading direction, and referred to as 1-2-B) have been addressed. Numerical models are defined by referring to composite FRP laminates having a rectangular shape (60 mm × 320 m) and comprising of eight plies, each one 1 mm thick. With reference to the loading direction (namely, x aligned along the long side of the laminate, see Fig. 7), two different stacking sequences are simulated: $[0]_{4s}$ and $[90]_{4s}$. Hole(s) in the laminate is (are) characterized by a diameter $D = 10$ mm, placed at the end-distance $E = 40$ mm (and with pitch $p = 40$ mm for double-bolted joints), and neat-fitting steel pin(s) is (are) considered.

Model geometries adopted for numerical simulations and some mesh details are depicted in Fig. 7, highlighting also the mesh refinement around the pin-plate interfaces, characterized by an average mesh size of about $5 \times 10^{-2} D$. Similarly to the validation case 2, as boundary conditions the pin center(s) is (are) assumed to be fully restrained, unilateral frictionless contact is considered at pin-plate interfaces, and an incremental displacement condition is enforced at the right laminate edge, with the displacement increment assumed equal to $0.5 \times 10^{-2} D$. Table 3 summarizes the values of model parameters employed for numerical computations.

5.2. Results and discussion

Figure 8 shows numerical results in terms of failure load values computed for the cases under investigation. As it is expected, results relevant to double-bolted joints exhibit greater values of the failure load with respect to the single-bolted joint configuration, with differences widely depending on the laminate stacking sequence and on the fiber material. In particular, the best strength performances are numerically experienced for the case $[0]_{4s}$, resulting

Table 3. Undamaged material properties and other model parameters employed for the comparative analysis described in Section 5. Matrix data are from [6]. Fiber data are from [29] for glass and basalt fibers, and from [30] for carbon fibers (T300 type). Pin properties are the same as in Table 1.

Fiber type	$S_f^{+/-}$ (GPa)	E_f^A (GPa)	E_f^T (GPa)	ν_f^T	ν_f^{AT}	G_f^{AT} (GPa)	V_f (%)
E-glass	1.90	74.0	74.0	0.22	0.22	30.3	60
Carbon	3.53	230.0	24.0	0.25	0.10	8.96	60
Basalt	2.95	90.0	90.0	0.26	0.26	35.7	60
Matrix	$S_m^{+/-}$ (MPa)	E_m (GPa)	ν_m	other	q_c	η_c	N
	26.0	1.4	0.4		3	100	10

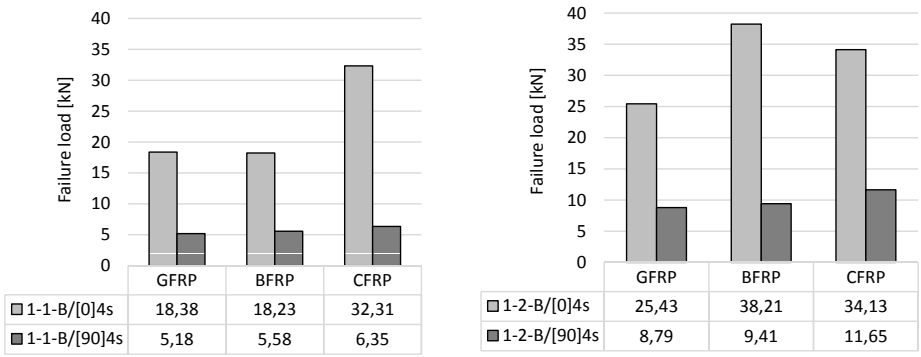

Fig. 8. Comparative analysis. Values of the failure load computed via the present model for single-bolted (1-1-B) and double-bolted joint configurations (1-2-B) defined in Fig. 7, and relevant to FRP laminates based on different fiber materials (glass, basalt, and carbon) and characterized by different stacking sequences.

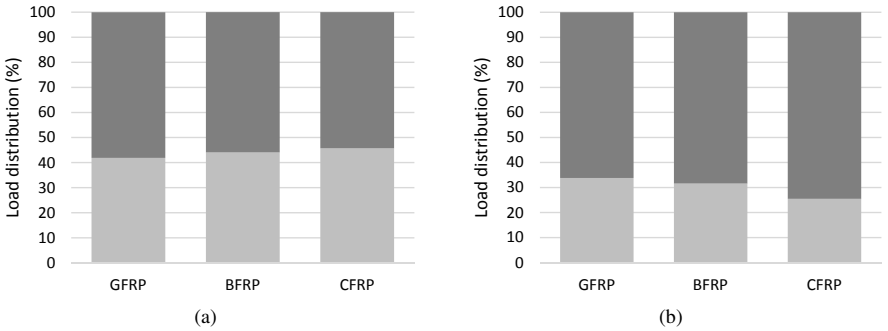

Fig. 9. Comparative analysis. Loading partition between the two pins for the 1-2-B joint configuration at the converged loading step just before the failure. (a) FRP laminates $[0]_{4s}$. (b) FRP laminates $[90]_{4s}$. Light gray: left pin (facing on the end-distance side). Dark gray: right pin.

for the 1-1-B-case in failure loads greater than the case $[90]_{4s}$ of more than 230 % for BFRP and GFRP, and of more than 400 % for CFRP (for 1-2-B, more than 180 % for GFRP and CFRP, more than 300 % for BFRP). It is worth pointing out that, failure loads computed for laminates $[90]_{4s}$ are almost similar, due to the little influence of the reinforcing fibers on the failure mode. Moreover, referring to the case $[0]_{4s}$ and for the joint configuration 1-1-B, failure loads computed for GFRP and BFRP are practically the same, whereas the use of carbon fibers allows one to obtain a double failure load than the GFRP and BFRP cases. On the other hand, numerical results computed for the double-bolted $[0]_{4s}$ configuration indicate that the use of basalt fibers yields a value of the failure load greater than that obtained addressing both GFRP (of about 50%) and CFRP (of about 11%). Such a result could be justified by observing that basalt fibers are characterized by a higher value of the transversal-to-fiber elastic modulus than carbon ones (see Table 3).

In the case of the double-bolted configuration, Fig. 9 highlights the load amounts (in percentage with respect to the total load), at the last equilibrated load-step (i.e., at the converged loading step just before the failure), carried by each pin. It is worth observing that, for laminates $[0]_{4s}$ the load is almost equally distributed between the two pins, resulting in a load carried by the left pin (i.e., for the pin facing on the end-distance side) of about 40-45 % (the smallest values for GFRP and the highest one for CFRP). On the contrary, when laminates $[90]_{4s}$ are investigated, the right pin carries about 65 % of the total load for GFRP and BFRP laminates, and 75% for CFRP.

Figures 10 and 11 depict at the failure state the equivalent von Mises stress patterns computed considering the different cases under investigation, with reference to 1-1-B (Fig. 10) and 1-2-B (Fig. 11) joint configurations. Correspondingly, Figs. 12 and 13 show the distributions of the equivalent material stiffness for the entire laminate along the

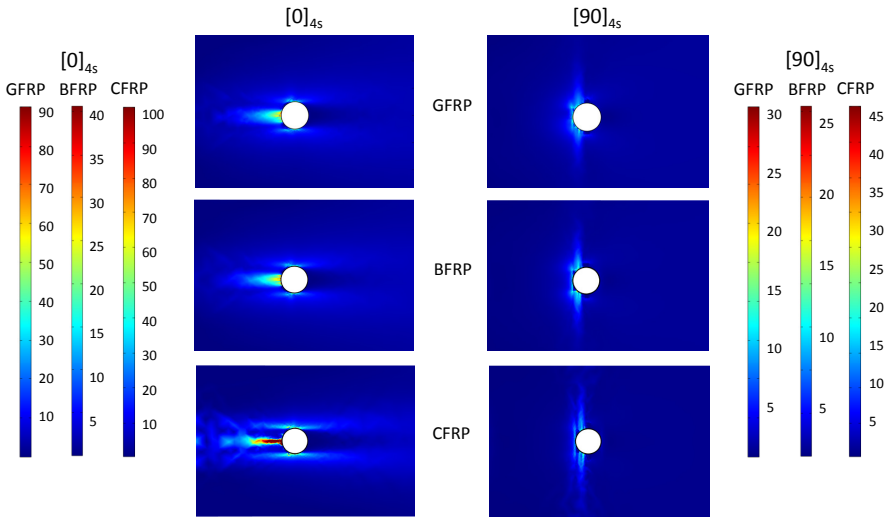

Fig. 10. Comparative analysis. Equivalent von Mises stress (in MPa) distribution at the failure state close to the pin-plate interface, for the 1-1-B joint configuration.

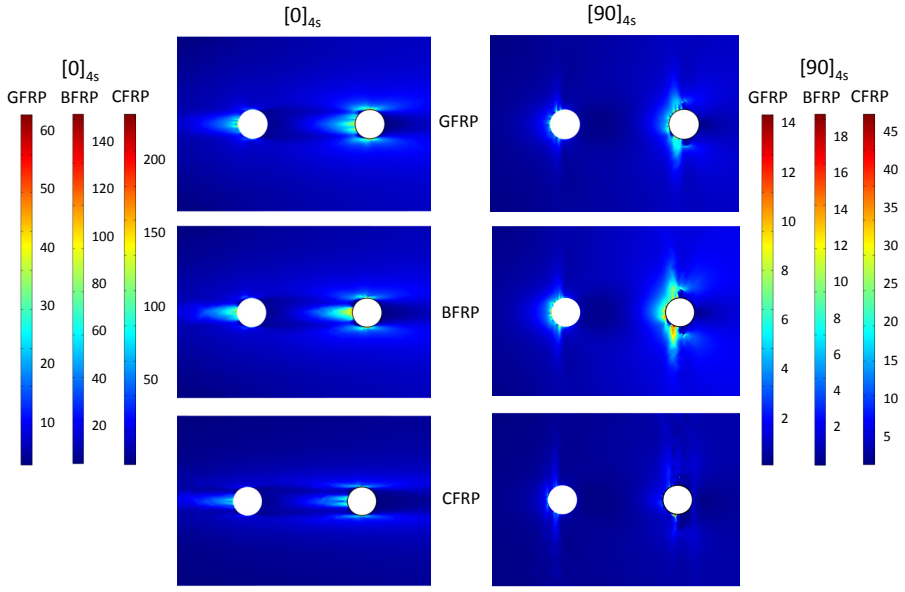

Fig. 11. Comparative analysis. Equivalent von Mises stress (in MPa) distribution at the failure state close to the pin-plate interfaces, for the 1-2-B joint configuration.

direction x (denoted as D_{xx}), providing an evidence of the damage localization mechanisms at the pin-plate interfaces (blue color indicates a fully damaged point, brownish red undamaged regions).

Proposed results clearly highlight that the failure mode for FRP laminates with a stacking sequence $[0]_{4s}$ is mainly based on a bearing mechanism, with dominant damage effects on the right pin for the 1-2-B joint configuration. On the contrary, when $[90]_{4s}$-laminates are addressed, a coupling between net-tension and bearing modes appears, resulting the net-tension failure mechanism as dominant for the right pin in the case 1-2-B, especially for CFRP laminates.

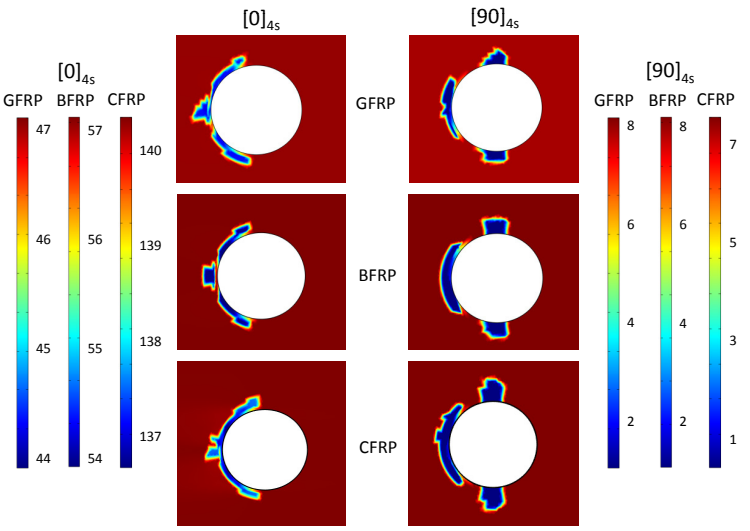

Fig. 12. Comparative analysis. Equivalent material stiffness (in GPa) of the entire laminate along the direction x (denoted as D_{xx}) at the failure state, close to the pin-plate interface and for the 1-1-B joint configuration.

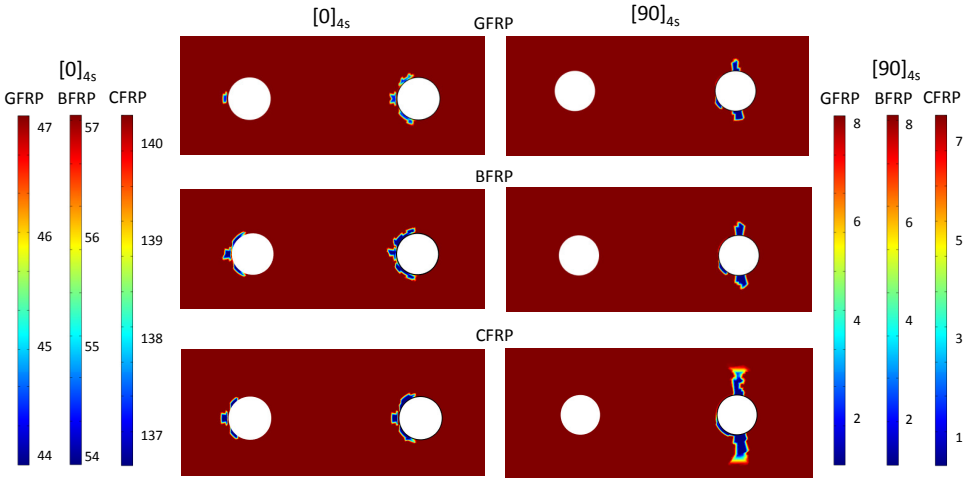

Fig. 13. Comparative analysis. Equivalent material stiffness (in GPa) of the entire laminate along the direction x (denoted as D_{xx}) at the failure state, close to the pin-plate interfaces and for the 1-2-B joint configuration.

6. Concluding remarks

The progressive damage occurring in bolted joints between fiber-reinforced composite laminates has been addressed, and an incremental nonlinear finite-element approach able to simulate failure mechanisms and damage localization in bolted laminates has been proposed. The model, based on a failure criterion that allows to account for micro-scale failure mechanisms (i.e., at the level of composite constituents), was formulated following a bi-dimensional plane-stress strategy and describing the contact at the pin-plate interfaces via a frictionless surface-to-surface penalty approach. Preliminary validation results based on experimental benchmarks available in literature have shown soundness and consistency of the proposed technique, resulting in simulated failure mechanisms and values of the failure load in good agreement with the experimental evidence. Moreover, the model has been applied to give comparative indications on the strength performance of FRP laminates when different reinforcing-fiber materials, number of pins,

and laminate stacking sequences are considered. In detail, reference is made to FRP laminates based on glass, basalt and carbon fibers, and by considering single- and double-bolted joint configurations.

Proposed numerical results have highlighted that the use of basalt fibers leads to failure loads fully comparable with those numerically-experienced in the case of glass fibers, although CFRP laminates with fibers mainly aligned along the carried-load direction exhibited the best performance in the case of single-bolted joints. Nevertheless, when two pins are considered along the loading direction and for laminates characterized by the stacking sequence $[0]_{4s}$, basalt fibers induced higher failure loads than both glass and carbon fibers. Moreover, discussed investigations seem to indicate that the use of basalt fibers in laminates with fiber not aligned along the loading direction tend to mitigate, with respect to the case of CFRP laminates, the occurrence of a net-tension failure mode as coupled with the bearing one, as a result of a much more balanced distribution of the carried load between the two pins.

These promising numerical evidence, together with the good physico-chemical qualities and low production cost, encourages further studies on basalt fibers as reinforcement constituents to be employed in effective connections among composite structural elements. In this framework, the proposed approach opens towards the possibility of simulating progressive damage mechanisms occurring in bolted joints between fiber-reinforced composite structural elements. Thereby, it could allow to provide useful contributions towards the definition of some technical guidelines for design and analysis of bolted connections for basalt-based FRP laminates.

Acknowledgements

This work was partially supported by the Italian Civil Protection Department [RELUIS-DPC 2014-18, CUP: E84G14000480007] and it was developed within the framework of the Lagrange Laboratory, a European research group comprising CNRS, CNR, the Universities of Rome Tor Vergata, Calabria, Cassino, Pavia and Salerno, Ecole Polytechnique, University of Montpellier II, ENPC, LCPC and ENTPE.

References

[1] F. Sen, M. Pakdil, O. Sayman, S. Benli, Experimental failure analysis of mechanically fastened joints with clearance in composite laminates under preload, Materials and Design 29 (2008) 1159–1169.
[2] F. Nerilli, L. Tarquini, M. Marino, G. Vairo, Numerical modeling of failure modes in bolted composite laminates, AIP Conference Proceedings 1648 (2015) 570019.
[3] M. McCarthy, V. Lawlor, W. Stanley, C. McCarthy, Bolt-hole clearance effects and strength criteria in single-bolt, single-lap, composite bolted joints, Composites Science and Technology 62 (2002) 1415–1431.
[4] Y.-G. Lee, E. Choi, S.-J. Yoon, Effect of geometric parameters on the mechanical behavior of PFRP single bolted connection, Composites Part B: Engineering 75 (2015) 1–10.
[5] U. Khashaba, T. Sebaey, K. Alnefaie, Failure and reliability analysis of pinned-joints composite laminates: Effects of stacking sequences, Composites Part B: Engineering 45 (2013) 1694–1703.
[6] F. Ascione, L. Feo, F. Maceri, An experimental investigation on the bearing failure load of glass fibre/epoxy laminates, Composites Part B: Engineering 40 (2009) 197–205.
[7] F. Ascione, L. Feo, F. Maceri, On the pin-bearing failure load of GFRP bolted laminates: An experimental analysis on the influence of bolt diameter, Composites Part B: Engineering 41 (2010) 482–490.
[8] A. Girão Coelho, J. Mottram, A review of the behaviour and analysis of bolted connections and joints in pultruded fibre reinforced polymers, Materials and Design 74 (2015) 86–107.
[9] S. Thoppul, J. Finegan, R. Gibson, Mechanics of mechanically fastened joints in polymer-matrix composite structures - A review, Composites Science and Technology 69 (2009) 301–329.
[10] L. Feo, G. Marra, A. Mosallam, Stress analysis of multi-bolted joints for FRP pultruded composite structures, Composite Structures 94 (2012) 3769–3780.
[11] A. Pisano, P. Fuschi, D. De Domenico, Failure modes prediction of multi-pin joints FRP laminates by limit analysis, Composites Part B: Engineering 46 (2013) 197–206.
[12] M. Swink, M. Sokolinsky, Continuous filament basalt fiber shows promise in high-temperature applications, International Fiber Journal 17 (2002) 52–56.
[13] B. Wei, H. Cao, S. Song, Environmental resistance and mechanical performance of basalt and glass fibers, Materials Science and Engineering: A 527 (2010) 4708–4715.
[14] K. Singha, A short review on basalt fiber, International Journal of Textile Science 1 (2012) 19–28.
[15] M. King, V. Srinivasan, T. Purushothaman, Basalt Fiber An Ancient Material for Innovative and Modern Application, Middle-East Journal of Scientific Research 22 (2014) 308–312.
[16] V. Fiore, T. Scalici, G. Di Bella, A. Valenza, A review on basalt fibre and its composites, Composites Part B: Engineering 74 (2015) 74–94.

[17] M. Marino, F. Nerilli, G. Vairo, A finite-element approach for the an alysis of pin-bearing failure of composite laminates, Fracture and Structural Integrity 29 (2014) 241–250.
[18] P. Dhè, Filament composed of basalt, US Patent 1438428 (1922).
[19] C. Colombo, L. Vergani, M. Burman, Static and fatigue characterisation of new basalt fibre reinforced composites, Composite Structures 94 (2012) 1165–1174.
[20] V. Lopresto, C. Leone, I. De Iorio, Mechanical characterisation of basalt fibre reinforced plastic, Composites Part B: Engineering 42 (2011) 717–723.
[21] Z. Wu, X. Wang, K. Iwashita, T. Sasaki, Y. Hamaguchi, Tensile fatigue behaviour of FRP and hybrid FRP sheets, Composites Part B: Engineering 41 (2010) 396–402.
[22] A. Dorigato, A. Pegoretti, Fatigue resistance of basalt fibers-reinforced laminates, Journal of Composite Materials 46 (2012) 1773–1785.
[23] L. Kollár, G. Springer, Mechanics of Composite Structures, Cambridge University Press, 2003.
[24] F. Auricchio, E. Sacco, G. Vairo, A mixed FSDT finite-element formulation for the analysis of composite laminates without shear correction factors, Lecture Notes in Applied and Computational Mechanics 23 (2005) 345–358.
[25] F. Auricchio, E. Sacco, G. Vairo, A mixed FSDT finite element for monoclinic laminated plates, Computers and Structures 84 (2006) 624–639.
[26] Z. Huang, A bridging model prediction of the ultimate strength of composite laminates subjected to biaxial loads, Composites Science and Technology 64 (2004) 395–448.
[27] A. Rotem, Predicxtion of laminate failure with the Rotem failure criterion, Composites Science and Technology 58 (1998) 1083–1094.
[28] F. Campbell, Structural Composite Materials, ASM International, 2010.
[29] KamennyVek, Advanced Basalt Fiber, 2014. URL: http://www.basfiber.com/about.
[30] TorayIndustries, Carbon Fibers America, Inc. (CFA), 2008. URL: http://www.toraycfa.com/pdfs/T300DataSheet.pdf.